

Three-dimensional Modeling of Vacuum Field Emission Nanotriodes

M. S. Khalifa,^{1,2} A. H. Badawi,^{1,*} T. A. Ali,^{1,2} N. H. Rafat,² and A. A. Abouelsaood²

¹*Center for Nanotechnology, Zewail City of Science and Technology, Giza 12588, Egypt*

²*Engineering Mathematics and Physics Department,*

Faculty of Engineering, Cairo University, Giza 12613, Egypt

Abstract

Vacuum nanodevices are devices that the electron transport through them is based on electron field emission from a nano-emitter to another opposite electrode through a vacuum channel. Geometrically asymmetric metal-vacuum-metal structures were demonstrated to have energy conversion ability for electromagnetic waves in the optical range. Combining the ability of these structures to convert optical signals into rectified current and the ability of vacuum nanotriodes to control the field emission current can allow direct processing on converted optical signals using a single device. In this paper, a three-dimensional quantum-mechanical method, rather than the approximate Fowler-Nordheim theory, is used for modeling the field emission process in vertical-type vacuum nanotriodes consisting of an emitter, a collector and a gate. The electron transport through the device is computed using a transfer-matrix technique. The potentials of vacuum nanotriodes in the current rectification and modulation are investigated at low voltages. The effects of varying the structure geometrical parameters on the rectified current are also studied. The obtained results show that a great enhancement in the rectification properties is achievable when the gate and the collector are connected through a DC source. It is also demonstrated that a small variation in the gate voltage can be used either to modulate the rectified current or to switch the device into a resonant tunneling diode.

I. INTRODUCTION

The rapid progress in nanofabrication during the past several years allowed for realizing nanostructures with minimum features of a few nanometers. This advancement, along with the growing need for high-frequency electronics, initiated the research in the field of vacuum nanoelectronics. Unlike semiconductor devices, vacuum nanoelectronic devices do not suffer from the limitation of electron velocity saturation as they depend on ballistic electron transport, which allows operating at higher frequencies. Also, they have greater thermal tolerance and exhibit higher robustness against high levels of radiation, which make them better candidates than semiconductor devices in extreme environments such as military and space applications. On the other hand, the active research in optical rectennas (rectifying nano-antennas) has recently exhibited promising results in energy conversion and current rectification. Combining the potentials of vacuum nanodevices with optical rectennas allows for fast, local modulation of the output current of rectennas. As a result, energy conversion, current rectification and processing functions can all be implemented by a single device. This opens the area to a wide field of applications in optical computing and communication technologies, where fast logic operations can be executed directly by rectennas.

In principle, vacuum nanoelectronic devices depend in their operation on field emission (FE) from nanotips supported on cathodes. The emitted electrons are usually collected at an opposite flat electrode (the anode or collector), and a gate may be added in the electrons path to control the magnitude of the emission current. Optical rectennas as well depend in their rectification behavior on asymmetric electrons emission (or tunneling) in asymmetric metal-insulator-metal (MIM) junctions. In this work we are particularly interested in vertical (Spindt-type) FE triodes¹. It was demonstrated that reducing the dimensions of the different parameters of such devices (tip radius, gate aperture diameter, and gap distance) is a key factor in enhancing their performance in terms of the current density, the applied voltages and the cutoff frequency^{2,3}.

Many attempts have been made in the process of miniaturizing these devices. In 1989, Brodie⁴ discussed the physics governing FE from a conic tip to an integrated collector electrode at a separation of distance $0.5 \mu\text{m}$, with gate aperture of radius $0.5 \mu\text{m}$. In 2000, Driskill-Smith et al.⁵ fabricated long nanopillars of radius 1 nm in a vacuum nano-chamber with dimensions of about $0.1 \mu\text{m}$. More recently, materials such as CNTs and Si nanowires have been used in fabrication as the emitting nanotips, for their high aspect ratio and relatively low operating voltages, with self-aligning gate around them⁶⁻¹⁰. This allowed minimizing the gate aperture down to 45 nm in radius³.

In Refs. 3–10, the authors described the FE process based on Fowler-Nordheim (FN) theory, in which the current density is expressed as a function of the electric field at the emitter surface. In the original FN theory, the emitting surface is assumed to be planar, and hence a one-dimensional problem is considered. This assumption is accurate as long as the emitter radius is much greater than the potential barrier, where the electric field can be considered uniform along the emitting surface. However, when the emitter radius is comparable to or smaller than the barrier width, the one-dimensional solution is no longer valid, and tunneling through a three-dimensional potential barrier should be considered instead. Although many correcting factors were introduced to FN basic equation for considering the emitter geometry and size^{11–14}, they were demonstrated to be inaccurate when applied to sharp emitters with radii $\lesssim 10$ nm¹². Another effective classical model, so called Quantum Corrected Model (QCM), was developed more recently for modeling electron tunneling through plasmonic nanogaps¹⁵. However, this model also assumes a potential barrier that is much smaller than the radius of the emitting surface, which is the typical case in plasmonic systems. For describing the behavior of vacuum nanotriodes without implying modeling restrictions, one can use either the Green-Function method^{16,17} or the Transfer-Matrix method^{18,19}. In each of these methods, Schrödinger’s equation is solved in three dimensions. In this work we follow the transfer-matrix method, which is more suitable in terms of memory storage when dealing with emitters with a few nanometers in height¹⁹.

In this paper, the model proposed by Mayer et al. in Ref. 20 for a high-frequency rectifier is extended by introducing a metallic gate to the structure for controlling the current flow through the device, so that the device resembles Spindt-type vacuum field emission triode. We mainly investigate the effect of the gate on the I-V characteristics of the device. We also study the effect of the gate voltage on the rectification properties of the device in the limit of quasi-static bias. In section II, we state the assumptions made in the model and present the method we follow in computing the potential energy distribution and the emission current, with emphasizing the modifications we introduced for considering the gate effect. The behavior of the device is then studied in section III. First, we present and discuss the modifications introduced to the potential barrier in the device due to the effect of the gate. Next, we investigate the possibility of improving the current rectification and the output power of the device in different situations for the gate potential. Then, we investigate the effect of the thickness, the height and the aperture diameter of the gate on the output current of the device. Finally, we investigate how changing the height and the diameter of the emitting tip can be exploited for improving the behavior of the device.

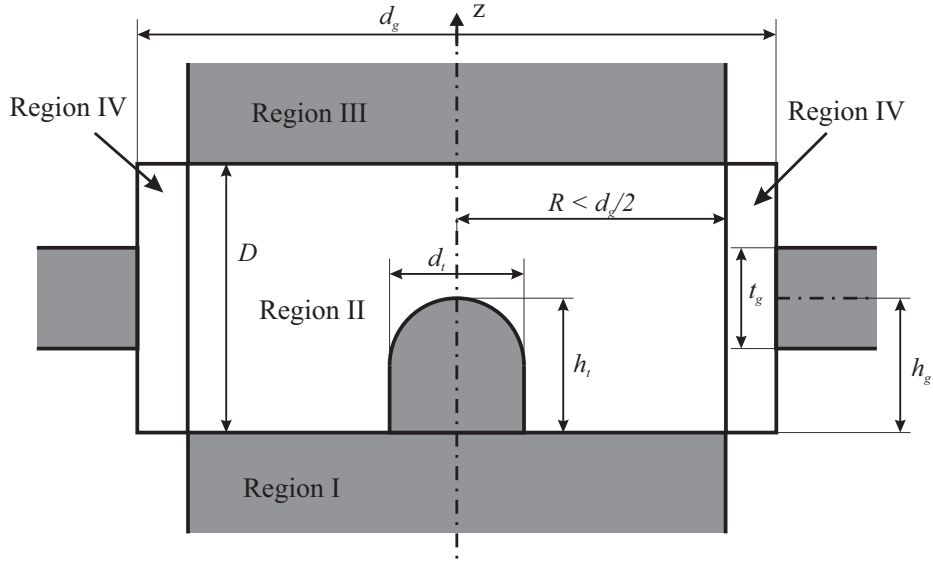


Figure 1: Schematic representation for the proposed structure. The rectangles at the sides represent the gate disc which surrounds the rectifier circularly, and are extended in the radial direction.

II. METHODOLOGY

A. Preliminaries

The structure we study in this paper is shown in Fig. 1. It consists of two metallic parallel flat planes separated by a distance D , with the lower one supporting a metallic cylindrical nanotip of a hemispherical end whose height and diameter are h_t and d_t , respectively. Similar structures with geometrical asymmetry were proven to exhibit rectification properties both theoretically^{20,21} and experimentally^{22–26}. A gate electrode, represented by an infinite horizontal metallic disc of thickness t_g , is set at height h_g above the lower metal, and contains a circular aperture of diameter d_g concentric with the tip. The rest of the space between the two surfaces is assumed to be vacuum.

We consider the metallic planes as two long leads (regions I and III) of radius R . The leads are assumed to be perfect conducting metals, that is, electrons inside them have a uniform potential energy. The objective of this section is to study the quantum transport between region I and region III through some quantum device (region II) representing the volume enclosed by the horizontal planes $z = 0$ and $z = D$, and the lateral surface defined by $\rho = R$. The vacuum cylindrical shell between the end of the leads at $\rho = R$ and the start of the gate at $\rho = d_g/2$ (region IV) is considered outside the device. Electrons are assumed to be confined in the leads and the device

within the cylindrical space of radius R , that is, the leakage current in the gate is neglected in this model and left for future investigations. This approximation is acceptable in the light of the results obtained by Driskill-Smith et al.⁵, where the calculations of the electrons trajectories showed that all electrons emitted from the tip are collected at the anode for all anode voltages except at zero volt.

We note here that R should not exceed the gate aperture radius, $d_g/2$, for two physical reasons. The first reason is that stacking three metallic layers with two vacuum barriers in between would result in resonant tunneling between the leads at the regions where the three layers overlap²⁷. This will then overwhelm the rectification behavior of the device as well as the current control by the gate. The second reason is to reduce the gate-cathode and the gate-anode capacitances that would decrease the cutoff frequency of the device¹⁰. In order to treat this situation in the analysis, we solve Poisson's equation in regions II and IV with taking the gate effect (both the potential on the gate as well as its metallic effect regardless of the metal type) as a boundary condition on the lateral edge of region IV at $\rho = d_g/2$ and at z between $h_g - t_g/2$ and $h_g + t_g/2$. Then we use the obtained value of the potential in region II only, where electrons are assumed to be localized, to solve Schrödinger's equation. The material properties of the gate, namely the workfunction and the Fermi energy, are not important in our calculations, because the leakage current is essentially assumed to be neglected, and the gate itself is taken outside the solution region which is limited by $\rho = R$.

When the structure is exposed to an external electric field directed along the axis of the device, z -direction, a potential difference is induced between the two leads with a magnitude that depends on the intensity of the field and the length of the device, D in Fig. 1, where $\Delta V = -ED$. This assumption is valid when considering an electrostatic field or a quasi-static electric field that could be carried by an incident electromagnetic wave with a relatively low frequency. The quasi-static limit here applies for waves whose periods are much longer than the average time an electron would take to transport through the device. For the structure parameters we consider in section III, the quasi-static limit is valid for small frequencies compared to 1000 THz²⁰. In all the upcoming analysis, we account for the external potential difference ΔV between the collector (upper lead) and the emitter (lower lead) by taking its value as a voltage applied to the collector; $V_c = \Delta V$, while the emitter is kept grounded. Similarly, we take the voltage applied to the gate V_g referred to the emitter.

B. Potential Energy Distribution

The first step in the analysis is obtaining the electron potential energy distribution in each of the four regions in Fig. 1 in order to solve Schrödinger's equation in regions I, II, and III accordingly. Metallic leads are considered in regions I and III with a work function W and a Fermi energy E_f . The electron potential energy in these regions are then $U^I = U^{III} = -(W + E_f)$. When external voltage V_c is applied to the upper lead, another term $-eV_c$ is added to the potential energy in region III, so that $U^{III} = -(W + E_f) - eV_c$, where e is the magnitude of the electron charge.

Unlike the previous two regions, regions II and IV include non-uniform potential energy distribution. Electron potential energy at any point in the vacuum in these regions consists of two parts; U_{bias} and U_{met} . The first part, U_{bias} , is the potential energy induced from the externally applied voltages on the leads and the gate. The electric potential distribution due to this bias, V_{bias} , can be obtained by solving Poisson's equation in the volume of regions II and IV, taking the following boundary conditions. In region II we take ground potential on the lower surface and the tip, and a constant potential V_c on the upper surface. In region IV, we take a zero charge boundary condition on the lower and the upper surfaces. On the lateral surface at $\rho = d_g/2$ there are three domains; a) $0 < z < h_g - t_g/2$, b) $h_g - t_g/2 < z < h_g + t_g/2$, and c) $h_g + t_g/2 < z < D$. The zero charge boundary condition is taken along the first and the third domains, while a constant potential V_g is taken along the second domain which represents the gate surface. The zero charge boundary condition indicates that the normal component of the electric field is zero at the boundary, i.e. the electric potential is constant along the normal direction. The second part, U_{met} , is the self-induced potential energy by the tunneling electron during its transport through the device. This part represents the potential energy of the electron due to the accumulated charges on the metallic surfaces of the leads, the tip and the gate. In this model, the electron image is taken on each metal surface individually as a first approximation. This enables calculating this part of the potential by solving Poisson's equation numerically^{28,29}, with the boundary condition $V_{met}(\mathbf{r}_b) = \frac{1}{4\pi\epsilon_0} \frac{e}{|\mathbf{r}_b - \mathbf{r}_e|}$ on all the metallic surfaces, including the gate, where \mathbf{r}_e is the position of the electron and \mathbf{r}_b is a point on the conductor at which the boundary potential is calculated. The zero charge boundary condition is taken here again on the non-metallic boundaries in region IV. The potential energy of the electron due to this electric potential is $U_{met}^{II}(\mathbf{r}_e) = -eV_{met}(\mathbf{r}_e)/2$, where the factor 1/2 arises from the fact that this potential energy is self-induced by the electron³⁰. In order to avoid the divergence of this term near the metallic surfaces, we cut all the values lower than the potential energy inside the metals and set them by this value^{31,32}. Since the metallic tip is supported on the

grounded lead, electrons in the tip have zero U_{bias}^{II} and constant $U_{met}^{II} = -(W + E_f^{tip})$, where E_f^{tip} is the Fermi energy of the material of the tip.

C. Field Emission Current

Now we proceed to solving Schrödinger's equation, using the obtained potential energy, in order to get the FE current. Since electrons are assumed to be confined in a cylinder of radius R , then their wavefunctions can be expanded in terms of complete, orthonormal eigenstates in cylindrical coordinates as follows¹⁸

$$\Psi(\rho, \phi, z) = \sum_{m,j} \Phi_{mj}(z) \frac{J_m(k_{mj}\rho)}{\sqrt{\int_0^R \rho [J_m(k_{mj}\rho)]^2 d\rho}} \frac{e^{im\phi}}{\sqrt{2\pi}} \quad (1)$$

where J_m is the m^{th} order of the Bessel function of the first kind, with m integer, and k_{mj} is the j^{th} coefficient satisfying $J'_m(k_{mj}R) = 0$, with j positive integer. $\Phi_{mj}(z)$ are the coefficients of the eigenstates depending on the coordinate z . In regions I and III, each lead has a constant potential energy and is considered semi-infinite in the z -direction, therefore for an electron with energy E the coefficients are $\Phi_{mj}^{I/III}(z) = \alpha e^{\pm ik_{z,mj}^{I/III} z}$, where $k_{z,mj}^{I/III} = \sqrt{\frac{2m_e}{\hbar^2} (E - U^{I/III}) - k_{mj}^2}$ and α is a normalization factor. The \pm sign indicates the propagation direction relative to z -axis.

To obtain the transmission probability through the quantum device (region II), the transfer-matrix method developed in Refs. 18, 19, and 33 is followed. In this technique the potential energy in region II is divided into two parts according to its coordinates-dependency; main potential $U_0^{II}(z)$ and local perturbing potential $U_1^{II}(\rho, \phi, z)$, such that $U^{II} = U_0^{II}(z) + U_1^{II}(\rho, \phi, z)$. After mathematical manipulations, a matrix equation coupling the coefficients $\Phi_{mj}(z)$ is obtained. Next, by discretizing region II into horizontal layers and assuming that U^{II} is independent of z inside each single layer, the matrix equation can be solved for all $\Phi_{mj}(z)$ in each layer, as illustrated in appendix A in Ref. 18. This enables calculating the scattering parameters for each layer individually. The scattering parameters of consecutive layers are then combined iteratively, using the layer addition algorithm^{19,34}, until one gets the total scattering parameters of region II.

Let S^{++} and S^{--} be the forward (from region I to III) and reverse (from region III to I) transmission matrices of the obtained scattering parameters. Then, the upward I^+ and the downward I^- electron currents can be obtained from the following expressions, respectively²⁰

$$I^+ = \frac{2e}{h} \int_{U_I}^{\infty} f_I(E) [1 - f_{III}(E)] \sum_{mj} \sum_{m'j'} \left| S_{(m',j'),(m,j)}^{++} \right|^2 \frac{k_{z_{m',j'}}^{III}}{k_{z_{mj}}^I} dE \quad (2)$$

$$I^- = \frac{2e}{h} \int_{U_{III}}^{\infty} f_{III}(E) [1 - f_I(E)] \sum_{mj} \sum_{m'j'} \left| S_{(m',j'),(m,j)}^{--} \right|^2 \frac{k_{z_{m',j'}}^I}{k_{z_{mj}}^{III}} dE \quad (3)$$

where $f_I(E)$ and $f_{III}(E)$ are the Fermi functions at regions I and III, whose Fermi levels are given by $\mu_I = -W$ and $\mu_{III} = -W - eV_c$, respectively. The temperature in the Fermi functions is taken to be 300 K.

For a finite number of modes and finite matrices dimensions, a finite number of values for the quantum numbers m and j should be considered. Ideally, all the values of m and j satisfying the relation

$$k_{mj} \leq \sqrt{\frac{2m_e}{\hbar^2} (E - \min(U^I, U^{III}))} \quad (4)$$

should be included. This condition ensures including all the modes propagating in at least one of the two leads, where these are the responsible modes for conducting current through the device. However, in the structure we study here, the existence of the tip around the z -axis makes the modes associated with small values of $|m|$ (the modes with high probability around the center) have higher contribution to the tunneling current than those associated with larger values of $|m|$. This is because the Bessel functions J_m have higher values near the center for smaller values of $|m|$,³⁵. This allows us to consider a) all modes with $|m| \leq m_{max}$, where m_{max} is as high as necessary for reaching convergence, and b) all values of j satisfying the above condition on k_{mj} for the associated m . In this work we take $m_{max} = 4$.

III. RESULTS AND DISCUSSION

In this section, we aim at exploring the potentials of the FE nanotriode for current rectification and modulation at low voltages. In particular, we investigate the effect of the gate in modulating the behavior of the structure and whether it can be exploited for enhancing the current rectification and the mean output power of the device. We also study how the geometrical parameters of the device affect its performance and how they can be optimized for current modulation through the gate voltage.

A. Potential Barrier Modulation

In this section, we study the effect of the gate on the shape of the potential barrier. We consider cylindrical leads with radius $R = 2$ nm, separated by distance $D = 2$ nm, as shown in Fig. 1, and made of tungsten whose work function and Fermi energy are 4.5 and 19.1 eV, respectively. In region II a nanotip of height $h_t = 1$ nm and diameter $d_t = 1$ nm is set on the lower lead, and made of tungsten as well. The rest of region II is assumed to be vacuum. Outside region II we consider a gate of thickness $t_g = 1$ nm set at height $h_g = 1$ nm above the lower lead, and aperture diameter $d_g = 4.1$ nm. The value of the gate aperture diameter is chosen to be greater than the leads diameter in order to avoid the resonant tunneling. Both the thickness and the height of the gate are chosen such that the gate is centered vertically at the end of the tip. Both the collector bias V_c and the gate bias V_g are taken to be 1 V. As we mentioned before in section II A, the material properties of the gate are not important in calculations, therefore all the results in this section are applicable to a gate of any metal that can be considered a perfect conductor.

According to the model assumptions in section II, the following results and discussion are applicable only to the limit of quasi-static fields. This limit depends on the cutoff frequency of the device, which is given by half of the reciprocal of the average time taken by an electron to travel between the emitter and the collector; the traversal time³⁶. In the classically forbidden region, an electron is assumed to be traveling at the Fermi velocity^{2,37}, while outside the barrier the electron propagates classically with a velocity that is proportional to its wavevector. Having the velocity and the gap distance between the emitter and the collector, the traversal time of the electrons can be calculated. For the structure parameters mentioned above, the traversal time takes a value of 0.5 fs²⁰, and the cutoff frequency is, therefore, 1000 THz, which corresponds to electromagnetic wavelength of about 300 nm, that is in the ultraviolet range. The quasi-static limit assumption is valid for frequencies significantly lower than this value. In case of oscillating fields with frequencies close to the cutoff frequency, photon absorption and emission should be included in the model^{38,39}. This problem will be treated in future work, including the gate voltage oscillation.

Due to the axial symmetry of the structure about the z -axis, electrons potential energy and hence their wavefunctions are independent of ϕ . Thus, it is sufficient to calculate the potential energy at a single plane defined by a certain ϕ . This allows calculating the bias potential V_{bias} at a single ρz -plane by solving Poisson's equation in two dimensions. In contrast, when calculating the image potential V_{met} , Poisson's equation is solved in three dimensions because the charge accumulation on the metallic surfaces is not axially symmetric for off-axis electron position. The

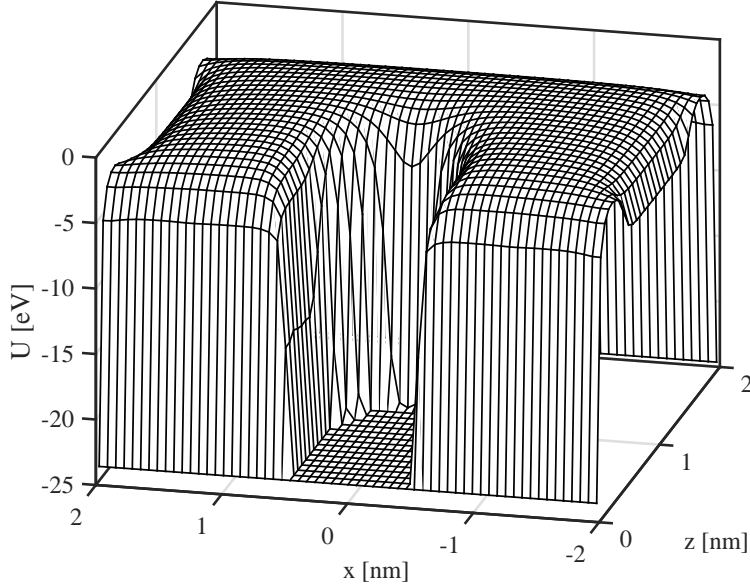


Figure 2: Potential energy distribution in xz -plane at equal collector and gate voltages of 1 V. The gate thickness t_g , height h_g and aperture diameter d_g are 1, 1 and 4.1 nm, respectively.

axial symmetry, however, can be exploited in calculating V_{met} by considering the electron positions in a definite ρz -plane (e.g. the xz -plane). Using COMSOL simulation tool, we calculate the two terms of the potential energy in region II; U_{bias}^{II} and U_{met}^{II} , as illustrated in section II B. The total potential energy distribution in region II, $U_{bias}^{II} + U_{met}^{II}$, is shown in Fig. 2. The corresponding potential barriers for electrons tunneling through the device at the lateral boundary ($\rho = 2$ nm) and at the center ($\rho = 0$) along the z -direction are drawn in solid lines in Figs. 3a and 3b, respectively. A potential well appears at $\rho = 2$ nm. This fast decrease in the potential energy distribution near the lateral boundary is mainly due to the image potential of the electron on the gate surface. The potential well may lead to resonant tunneling, specifically if one or more of the resonant energies are around the Fermi level of the emitter. If the minimum resonant energy is, however, significantly larger than the Fermi level of the emitter, no considerable resonant tunneling occurs because the electrons occupation for resonant energies is almost zero. The resonant tunneling effect, as mentioned before, is undesirable because it leads to high level of conduction in both directions which reduces the rectification effect of the tip.

It is interesting to see how changing the gate voltage would modulate the shape of the barrier and the well. Fig. 3 shows the potential energy along z -axis for four different values of V_g ; -1 , 1 , 3 and 5 V, at both $\rho = 2$ nm (a) and $\rho = 0$ (b). These voltages are chosen to show the barrier

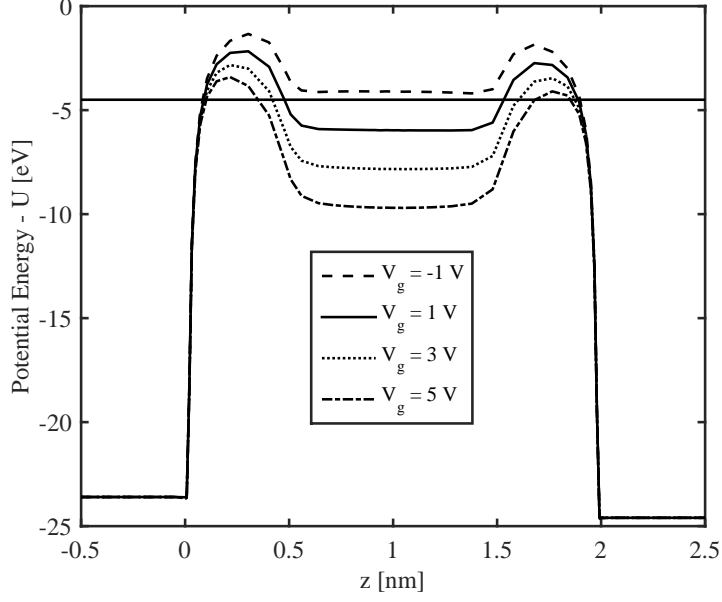
modulation around the Fermi level near the edge. As the gate voltage increases the depth of the well at the edge increases, while the potential barrier at the center slightly decreases. The increasing depth of the well results in decreasing the resonant energy levels down to the vicinity of the Fermi level. Although the resonant tunneling effect is not favorable from the rectification point of view, the dependence of the well depth and the resonant levels on the gate voltage may be useful from another perspective, where the device can operate as a resonant tunneling diode with controllable potential well. The more interesting part is that with only changing the gate voltage the device can be switched between the rectification mode and the resonant tunneling mode. As shown in Fig. 3a at $V_g = -1$ V, the Fermi level is totally buried under the potential energy along the z -axis, which means that there is no chance for resonant tunneling to occur. However, a more comprehensive study for the device in the case of resonant tunneling is still needed, which is beyond the scope of this paper.

The peaks of the potential energy curves at $\rho = 0$ are magnified in the inset in Fig. 3b in order to show the small changes in the barrier height and width at different gate voltages. As the gate voltage increases, the barrier gets slightly lower and narrower. These small changes indicate that the effect of the gate significantly decays as we go from the lateral boundary inwards until it is minimally pronounced at the center.

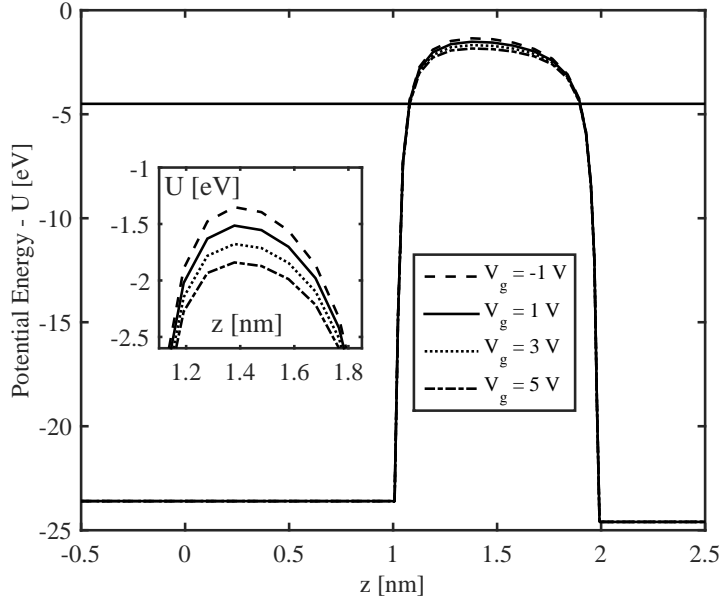
In order to investigate the effect of the gate aperture diameter d_g , we repeated the above calculations for $d_g = 4.5$ nm. The potential energies at the lateral boundary are depicted in Fig. 4. The image potential on the gate surface almost vanished when the gate diameter increased from 4.1 to 4.5 nm. This result caused the potential well to totally disappear at gate voltages lower than 5 V, which means that the gate voltage can reach higher values without the device encountering resonant tunneling. Regarding the potential barrier at $\rho = 0$, there is no significant difference due to increasing d_g except for a slight decrease in the change of the potential barrier with changing the gate voltage.

The current-voltage characteristics of a device of the previous parameters at the cases of $V_g = -1$ and 1 V are shown in Fig. 5. The results show the current modulation effect associated with the barrier modulation, while keeping the rectification nature of the device. This demonstrates the possibility of implementing electronic processes directly on the rectified current through applying a gate voltage of a few volts in magnitude. Both the rectification and the modulation abilities of the device are discussed in more detail in the following two sections.

Finally, we note that the width and the position of the well along the z -axis at $\rho = 2$ nm can



(a)



(b)

Figure 3: Potential energy along z -axis at (a) $\rho = 2$ nm and (b) $\rho = 0$ when $V_c = 1$ V and $V_g = -1, 1, 3$ and 5 V. The peak of the barrier at $\rho = 0$ is magnified in the inset in (b) in order to show small changes in the barrier height at different gate voltages. The gate thickness t_g , height h_g and aperture diameter d_g are $1, 1$ and 4.1 nm, respectively. The horizontal black solid lines indicate the Fermi level inside the emitter.

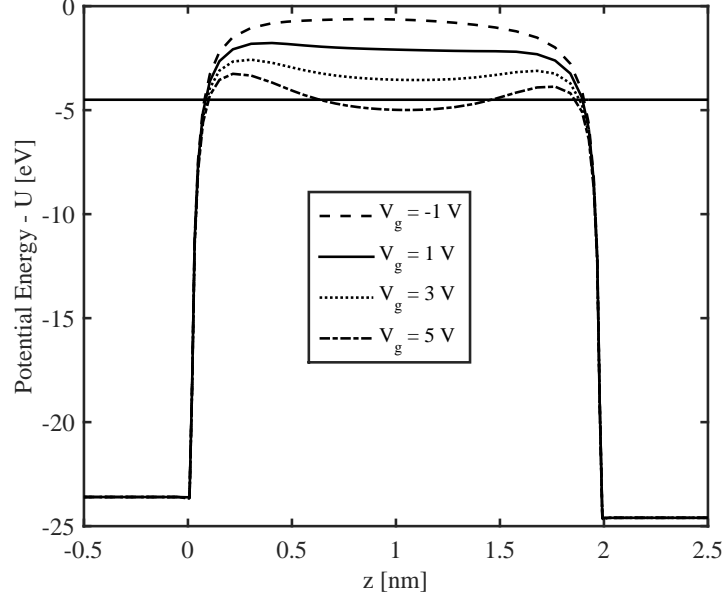


Figure 4: Potential energy along z -axis at $\rho = 2$ nm when $V_c = 1$ V and $V_g = -1, 1, 3$ and 5 V. The gate thickness t_g , height h_g and aperture diameter d_g are 1, 1 and 4.5 nm, respectively. The horizontal black solid line indicates the Fermi level inside the emitter.

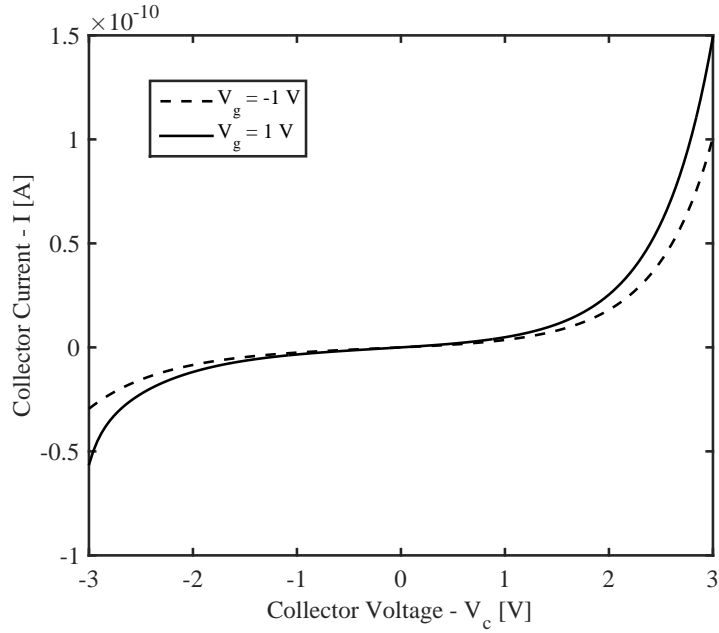


Figure 5: Current-voltage characteristics of the triode at $V_g = \pm 1$ V. The gate thickness t_g , height h_g and aperture diameter d_g are 1, 1 and 4.5 nm, respectively.

be controlled by the thickness and the height of the gate, respectively. Similar to the dependence of the depth of the well on the gate voltage, the dependence of the width of the well on the gate thickness fades away as the gate aperture diameter increases. A more detailed investigation for the effect of the gate thickness and height is presented in section III C.

B. Gate Effect on Current Rectification and Modulation

In this section, we investigate how the existence of the gate modifies the rectification properties of the device. We are interested here in calculating both the forward and backward currents. For a positive external bias V_c , the forward current is given by $I_{fwd} = I^+ - I^-$, while for a negative external bias, the backward current is given by $I_{bwd} = I^- - I^+$, where I^+ and I^- are the upward and downward currents whose expressions were given in Eqs. (2) and (3), respectively. The ability of the device to deliver a higher current in the forward bias than the backward when subject to the same absolute value V_c is measured by the rectification ratio $Rect = I_{fwd}/I_{bwd}$. If an oscillating field of a frequency significantly lower than the cutoff frequency is incident on the device, an oscillating potential difference of magnitude V_c is induced between the collector and the emitter. The device is then supposed to deliver an asymmetric oscillating current between I_{fwd} and $-I_{bwd}$. This indicates that when operating as a power source, the device is capable of delivering an output DC power given by $\langle P \rangle = \frac{1}{2}V_c(I_{fwd} - I_{bwd}) = \frac{1}{2}V_c I_{fwd}(1 - 1/Rect)^{20}$. From this expression, we see that the output power can be optimized by increasing the forward current and the rectification ratio.

We now consider three cases for the gate connection; a) the gate is connected through a DC source V_{DC} to the emitter, b) the gate is connected through a DC source V_{DC} to the collector, and c) the gate has a floating potential. In the first two cases we consider three values for V_{DC} : 2 V, 0 and -2 V. This corresponds to $V_g = 2$ V, 0 and -2 V in the first case, and $V_g = V_c + 2$ V, V_c and $V_c - 2$ V in the second case. Since we are targeting low voltages, the two values 2 and -2 V are taken as the extremes of the spanning range of V_{DC} . In the following results we consider the same geometrical parameters mentioned in section III A with $d_g = 4.5$ nm. Since the gate electrode is centered at the midpoint between the collector and the emitter, therefore in the third case the floating gate voltage is driven to the mid-value between their voltages ($V_g \approx V_c/2$).

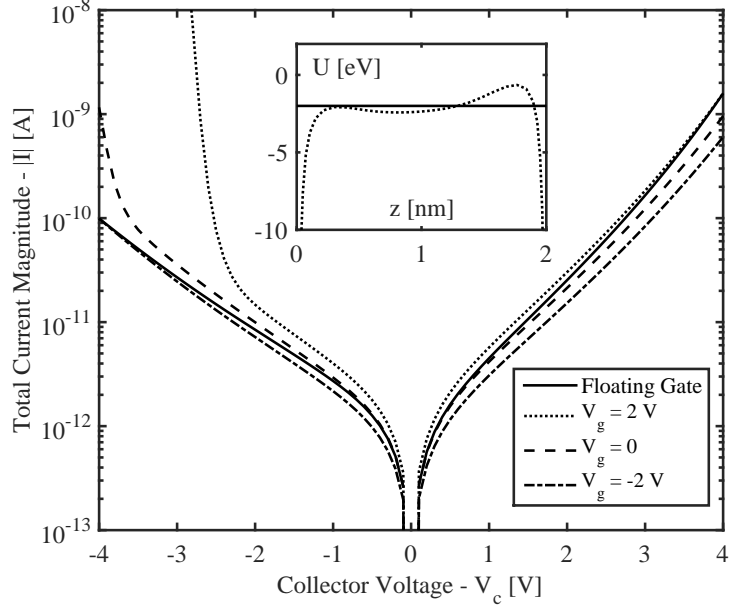
Figs. 6a and 6b show the magnitudes of the currents versus the collector voltage for the three values of V_{DC} in cases (a) and (b) of the gate connection, respectively. The magnitude of the current in case (c), where the gate potential is floating, is included in both figures as a reference.

The collector voltage is varied from -4 to 4 V, which corresponds to applying electric fields of magnitudes between 0 and 2 Vnm $^{-1}$ on the device along the z -direction.

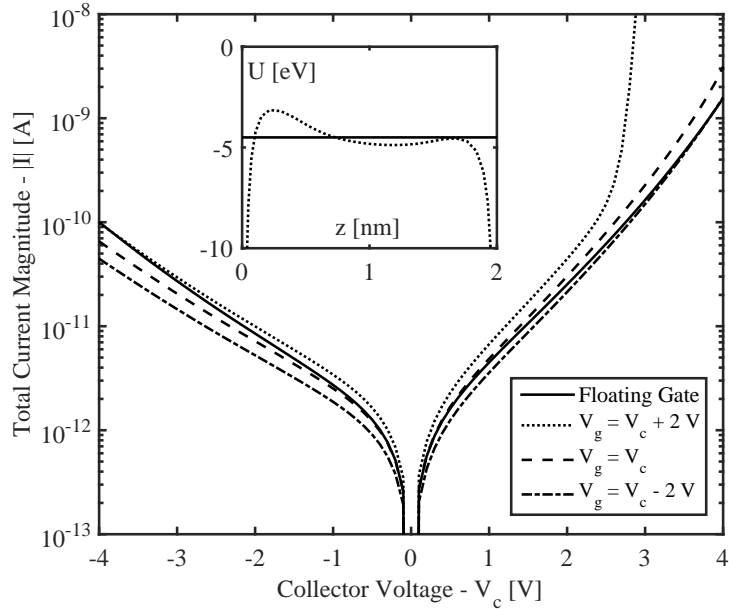
In the case of the floating gate potential, no difference is observed in both forward and backward currents from the original case, in which no gate existed. In order to understand the results of the other gate connections, we refer to the results of the floating gate potential as the reference results. We also refer to the self-biased gate voltage in this case, which is $V_c/2$, as the gate reference voltage V_{ref} . At V_g greater than the reference voltage, the barrier drops below its reference height (its height when the gate voltage is floating). So, the current increases such that if V_c is positive the forward current increases, while if it is negative the backward current increases. At $V_g < V_{ref}$, the barrier rises above its reference height and the current decreases. If the vertical position of the gate is changed between the emitter and the collector, the reference voltage will change. For example, if the gate is centered around $3/4$ of the distance D between the emitter and the collector, then the gate reference voltage will be $\frac{3}{4}V_c$, above which the current increases and below which the current decreases, keeping its direction controlled by V_c polarity.

Based on this argument the results in Fig. 6 can be explained. In the case when the gate is connected directly to the emitter ($V_g = 0$), the gate voltage is lower than the reference voltage for a positive V_c , while it is higher than it for a negative V_c . Thus, the forward current is lower than the reference forward current, and the backward current is higher than the reference backward current. At $V_g = -2$ V, the reference voltage is greater than the gate voltage as long as V_c is greater than -4 V (because $V_{ref} = V_c/2$), and therefore the current magnitude is lower than the reference current. Exactly at $V_c = -4$ V, the two curves intersect. For lower values of V_c the backward current of $V_g = -2$ V exceeds the reference backward current. Similarly, at $V_g = 2$ V the current curve intersects with the reference current at $V_c = 4$ V. However, in this case the backward current increases dramatically at collector voltages below -2.5 V. This is because the Fermi level in the emitting electrode (the collector in this case) raised above one of the vacuum barriers at $\rho = 2$ nm (see the inset in Fig. 6a). Electrons at the Fermi level, thus, encounter a single narrow barrier, which increases their tunneling probability. As the collector voltage decreases, the Fermi level inside the collector increases leading to a narrower barrier and hence a higher backward current. Such an increase in the current occurs when the gate potential is large compared to the potential of the emitting electrode. This effect can be used for switching the current on and off by varying the gate potential only, ignoring the rectification effect.

In a similar manner, the current curves when the gate is connected to the collector through a



(a)



(b)

Figure 6: Current magnitude versus collector voltage at different gate connections. The gate is connected through a DC source of values 2, 0 and -2 V to the emitter in (a) and to the collector in (b). The insets show the potential energy along the z -direction at $\rho = 2$ nm, when $V_c = -2.5$ V and $V_g = 2$ V in (a), and when $V_c = 2.5$ V and $V_g = V_c + 2$ V = 4.5 V in (b). The horizontal solid lines in the insets indicate the Fermi level in the emitting electrode (the collector in (a) and the emitter in (b)).

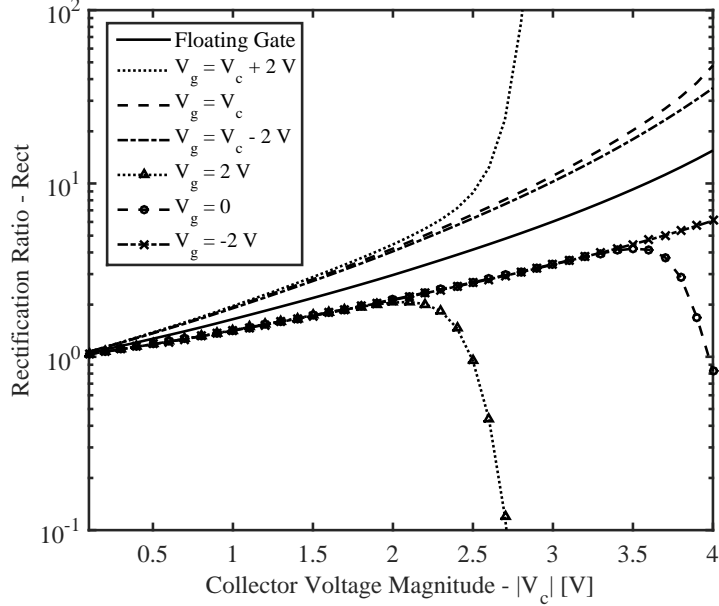


Figure 7: Rectification ratio at the different gate connections. The ratio is calculated for the forward and backward currents in Fig. 6.

DC source in Fig. 6b can be understood. In this case, however, all the effects are reversed. For example, at $V_g = V_c$ the forward current increases over its reference value, while the backward current is suppressed. The potential energy profile in this case is the same as if a single electrode of applied voltage V_c is extended from the collector to the gate along the outer side of region IV. This structure represents a diode of inverted U-shaped (or concave) collector. The obtained current results then imply that such a diode shall have enhanced rectification properties over the original diode of a flat collector.

At $V_g = V_c + 2 \text{ V}$, the forward current increases dramatically at collector voltages above 2.5 V in an analogous way to the increase of the backward current at $V_g = 2 \text{ V}$. This time, however, the increase in the current is in favor of the rectification behavior of the device. We note that in both cases this effect appears when the difference between the gate voltage and the emitting electrode voltage is around 4.5 V, which is the value of the work function of the metal.

The rectification ratio and the magnitude of the output power for the different gate connections are presented in Figs. 7 and 8, respectively. The results show that both the rectification ratio and the output power are enhanced, compared to the floating gate situation, when the gate is connected directly to the collector, while they deteriorate when the gate is connected to the emitter through a DC source.

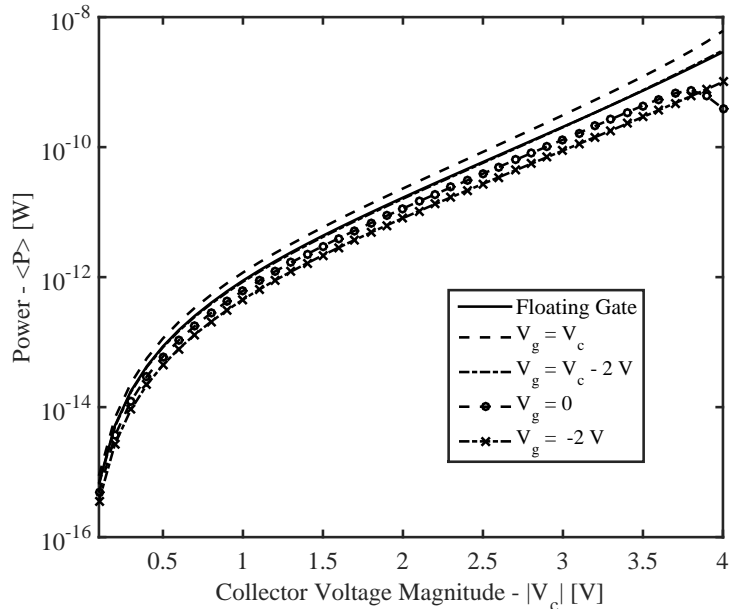


Figure 8: Output power at the different gate connections. The power is calculated for the corresponding forward and backward currents in Fig. 6.

In the conclusion of this section we can summarize how the gate electrode can be exploited to enhance the output power of the device. In order to increase the forward current, the gate voltage should be greater than the reference voltage, however this may also increase the backward current even higher and result in decreasing the rectification ratio. On the other hand, to increase the rectification ratio the gate should have a DC value referred to the collector not the emitter. This means that it should be connected to the collector with DC shift, that is $V_g = V_c + V_{DC}$ with respect to the emitter. Combining the previous two results, the output power can be enhanced by connecting the gate to the collector through DC source whose value is larger than negative the difference between V_c and the reference voltage ($V_{DC} > -(V_c - V_{ref})$). As V_{DC} increases, forward current, rectification ratio and the mean output power will increase. However, it should not increase much above zero to avoid resonant tunneling.

There is one remaining note regarding the validity of the model assumptions in power calculations. Since the leakage current in the gate is neglected, there is no power consumed or delivered through the gate electrode. In practice, however, this approximation is not very accurate, particularly in the case of high gate voltages, where any small current leakage in the gate would result in considerable power exchange through it. If the device is to be used in energy conversion applications, gate current should be included in power calculations, otherwise the calculated power

efficiency of the device would be misleading.

C. Dependence of the Collector Current Modulation on the Gate Parameters

In this section, we investigate the ability of the nanotriode to modulate the collector current using the gate voltage, and the modulation dependence on the geometrical parameters of the gate. The collector voltage is fixed at 1 V, and only the forward current is considered in the calculations. We take values of V_g between -2 and 2 V. All the geometrical parameters are similar to section III A except that the gate aperture diameter is 4.2 nm. This diameter is big enough to avoid resonant tunneling at the maximum gate voltage value used in this section (2 V).

We start with the effect of the gate thickness t_g on the triode's ability to alter the current through the gate voltage V_g . Fig. 9 shows the forward current as a function of the gate voltage at four different gate thicknesses. Since we are interested in studying the nanotriode in its smallest practical dimensions, we consider the smallest possible thickness for a monolayer conducting sheet. This is estimated to be in the range of 0.35 nm for a graphene layer^{40,41}. On the upper limit, we are restricted by the separation between the collector and the emitter. A gate with thickness approaching this separation would result in high-probability tunneling between the emitter and the collector through the gate, turning the device into a conductor. Structures with non-flat gate, such as tapered gate, around the tip will be studied in future work. Fig. 9 shows that as the gate thickness increases, the variation of the current with the gate voltage increases. At a gate thickness of 1.4 nm, an increase in the gate voltage from -2 to 2 V causes an increase in the current by 130%.

Turning to the effect of the vertical position of the gate, we present the current results at gate thickness of 0.7 nm for three different gate positions in Fig. 10. The three positions are chosen such that a) the gate is just above the tip end ($h_g = 1.35$ nm), b) the gate is centered around the tip end ($h_g = 1$ nm), and c) the gate is surrounding the highest part of the tip ($h_g = 0.65$ nm). It is obvious from the results that the largest variation in the current is obtained when the gate is centered around the end of the tip. That is because the highest part in the potential barrier at any radial position within the tip range is just above its curved surface, so the gate is most effective when centered around this region. The results in Fig. 10 also show that the current variation is minimal in the third case when $h_g = 0.65$ nm. That is because the gate is the furthest from the barrier between the end of the tip and the collector surface at the center of the device ($\rho = 0$) where the tunneling current density is the maximum.

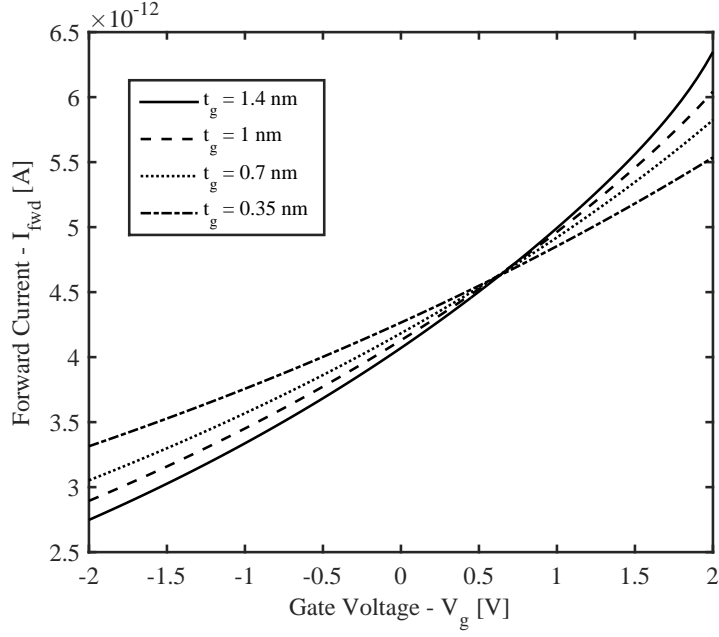


Figure 9: Forward current versus gate voltage at collector voltage V_c of 1 V for four different values of gate thickness; $t_g = 1.4, 1, 0.7$ and 0.35 nm. The gate height h_g and aperture diameter d_g are 1 and 4.2 nm, respectively.

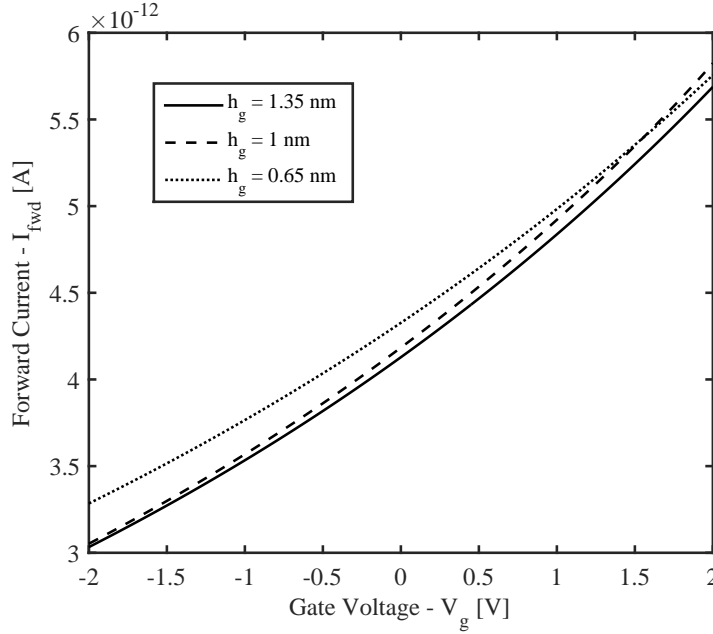


Figure 10: Forward current versus gate voltage at collector voltage V_c of 1 V and gate thickness t_g of 0.7 nm for three different heights of the gate; $h_g = 1.35, 1$ and 0.65 nm. The gate aperture diameter d_g is 4.2 nm. The chosen three heights correspond, descendingly, to the positions of the gate where it is just above, centered around, and just below the end of the tip.

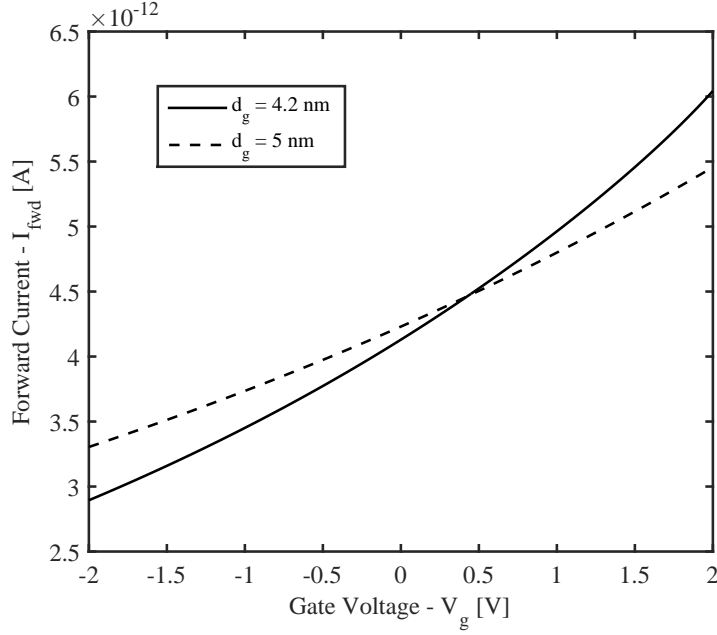


Figure 11: Forward current versus gate voltage at collector voltage V_g of 1 V and gate thickness t_g of 1 nm for two different gate aperture diameters; 4.2 and 5 nm. The height of the gate is 1 nm.

The effect of the gate aperture diameter on the shape of the potential barrier is discussed in section III A. Now we investigate how this dependency will affect the variation of the current with varying the gate voltage. Fig. 11 shows the $I - V_g$ relation for gates of aperture diameters 4.2 and 5 nm. The gates considered here have a thickness and a height of 1 nm. The decrease of the current variation with increasing the aperture diameter is clear from the graph. This result is quite predictable from the potential energy results in Figs. 3 and 4.

D. Dependence of Current Modulation on the Tip Parameters

In Refs. 20 and 42, Mayer et al. demonstrated that better rectification properties are for emitting tips with higher aspect ratio. With adding the gate electrode to the structure, we aim in this section at investigating the effect of the aspect ratio on current modulation. In this section we use gate thickness, height and aperture diameter of 1, 1 and 4.2 nm, respectively. As shown in Fig. 12, by increasing the tip diameter d_t from 1 to 1.5 nm at the same tip height ($h_t = 1$ nm), an increase in both the average current and the slope of the $I - V_g$ curve is observed. The increase in the average current value is due to the increase of the emitting area represented by the tip surface. Such an increase in the forward current is necessarily accompanied by a higher increase in the backward current, due to the decreasing field enhancement, resulting at the end in reducing

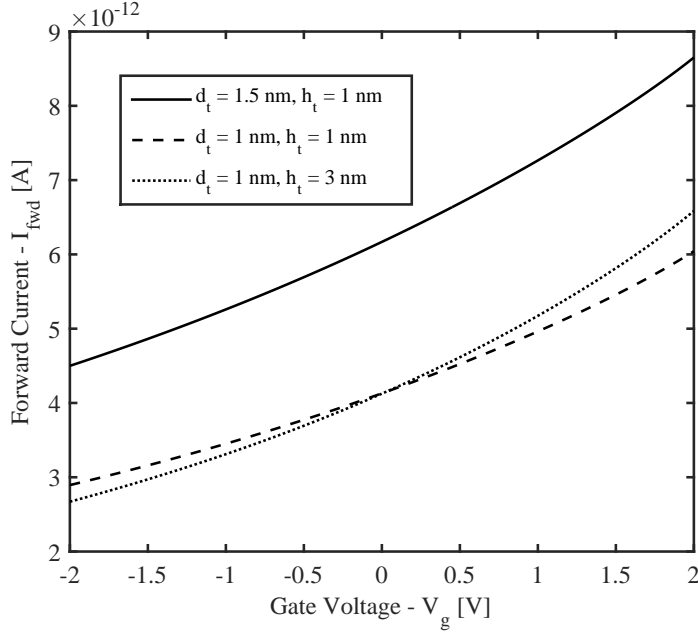


Figure 12: Forward current versus gate voltage at collector voltage V_c of 1 V for different tip parameters. At the two cases where $h_t = 1$ nm, the separation distance between the leads D is 2 nm. At $h_t = 3$ nm, $D = 3$ nm. In the three cases, the gate thickness t_g and aperture diameter d_g are 1 and 4.2 nm, respectively, and $h_g = h_t$.

the rectification ratio. The increase in the slope is mainly because the emitting tip extended to a closer region to the gate, where the modulating effect is more significant on the potential energy and the emitted current.

Finally, we investigate the gate modulation effect on tips of different heights. A tip of height 3 nm and diameter 1 nm is examined. The separation between the leads is 4 nm, so that the width of the potential barrier between the tip and the collector is 1 nm as in the previous cases. Also the gate is set at height of 3 nm, in order to be centered around the end of the tip as well. A better current modulation is observed at this higher tip (dotted curve in Fig. 12). This result exhibits a favorable behavior for the device due to its compatibility with the results obtained in Refs. 20 and 42, where optimized rectification properties were also demonstrated for higher tips.

IV. CONCLUSION

In this paper, a transfer matrix method is used to model quantum tunneling through vacuum nanotriodes at low applied voltages. The structure consists of a metal-vacuum-metal junction with a nanotip supported on one of the metals and surrounded by a thin gate electrode. The device

resembles Spindt-type vacuum triodes with a collector-emitter separation and a gate aperture diameter of a few nanometers. The details of calculating the potential energy distribution and the field emission current are presented with considering the gate effect. The behavior of the device is then investigated as a current rectifier and modulator at different electric and geometric parameters.

The results show a significant enhancement in the rectification properties of the geometrically asymmetric metal-vacuum-metal diode when a gate electrode is connected to the collector through a DC source. This finding suggests a better rectification for vacuum nanodiodes with concave collectors instead of flat ones. It is also demonstrated that the output current of the device can be modulated by the gate voltage. The effect of the geometrical parameters of the gate and the tip on current modulation are investigated. It is shown that a gate centered around the end of the tip with a narrow aperture and a large thickness gives the best current modulation. It is also shown that the currents emitted from tips of higher aspect ratios are better controlled through the gate potential. In order to achieve electric currents of higher magnitudes at the same applied potentials, we have to either decrease the gap distance between the emitting tip and the collecting surface, or increase the emitting surface area. The second solution can be realized by adding more than one nanotip or a protruding ring. Such structures can be designed and characterized following the same approach we present in this work. However, in order for this model to be fully reliable in the design and the characterization processes, experimental verification on similar dimensions is needed.

Based on this analysis, the vacuum nanotriode we study in this paper represents an excellent candidate for high-frequency applications. It can be optimized to do the basic functions of transistors, in addition to its rectification effect, at high frequencies up to the infrared range. Thus, it is a possible alternative to semiconductor transistors as a basic unit in electronic circuits. It can also be used for implementing local processing operations on rectennas, avoiding the transmission problems of high-frequency signals. This shall open the door to a new era of fast electronics, where communication systems and processing units operating at optical frequencies are achievable. It can also be used as an electronic interface for plasmonic circuits.

ACKNOWLEDGMENTS

M. Khalifa would like to thank A. Mayer for his valuable comments and suggestions.

* Corresponding author; abadawi@zewailcity.edu.eg

- ¹ C. A. Spindt, *Journal of Applied Physics* **39**, 3504 (1968).
- ² H. Q. Nguyen, P. H. Cutler, T. E. Feuchtwang, Z. H. Huang, Y. Kuk, P. J. Silverman, A. A. Lucas, and T. E. Sullivan, *IEEE Transactions on Electron Devices* **36**, 2671 (1989).
- ³ P. Y. Chen, H. Huang, D. Akinwande, and A. Alù, *IEEE Transactions on Nanotechnology* **11**, 1201 (2012).
- ⁴ I. Brodie, *IEEE Transactions on Electron Devices* **36**, 2641 (1989).
- ⁵ A. A. G. Driskill-Smith, D. G. Hasko, and H. Ahmed, *Journal of Vacuum Science & Technology B* **18**, 3481 (2000).
- ⁶ D. G. Pflug, M. Schattenburg, H. I. Smith, and A. I. Akinwande, *International Electron Devices Meeting. Technical Digest (Cat. No.01CH37224)*, 8.5.1 (2001).
- ⁷ M. A. Guillorn, A. V. Melechko, V. I. Merkulov, E. D. Ellis, C. L. Britton, M. L. Simpson, D. H. Lowndes, and L. R. Baylor, *Applied Physics Letters* **79**, 3506 (2001).
- ⁸ L. Ganaloff, E. Minoux, K. B. K. Teo, P. Vincent, V. T. Semet, V. T. Binh, M. H. Yang, I. Y. Y. Bu, R. G. Lacerda, G. Pirio, J. P. Schnell, D. Pribat, D. G. Hasko, G. A. J. Amaratunga, W. I. Milne, and P. Legagneux, *Nano Letters* **4**, 1575 (2004).
- ⁹ Y. M. Wong, W. P. Kang, J. L. Davidson, B. K. Choi, W. Hofmeister, and J. H. Huang, *Diamond and Related Materials* **14**, 2069 (2005).
- ¹⁰ G. Ulisse, F. Brunetti, F. Ricci, A. M. Fiorello, and A. D. Carlo, *IEEE Electron Device Letters* **33**, 1318 (2012).
- ¹¹ Jun He, P. H. Cutler, N. M. Miskovsky, T. E. Feuchtwang, T. E. Sullivan, and Moon Chung, *Surface Science* **246**, 348 (1991).
- ¹² P. H. Cutler, J. He, N. M. Miskovsky, T. E. Sullivan, and B. Weiss, *Progress in Surface Science* **42**, 169 (1993).
- ¹³ K. L. Jensen and E. G. Zaidman, *Journal of Vacuum Science & Technology B* **13**, 511 (1995).
- ¹⁴ D. Nicolaescu, V. Filip, S. Kanemaru, and J. Itoh, *IVMC 2001. Proceedings of the 14th International Vacuum Microelectronics Conference (Cat. No.01TH8586)* **21**, 366 (2003).

- ¹⁵ R. Esteban, A. G. Borisov, P. Nordlander, and J. Aizpurua, *Nature Communications* **3**, 825 (2012).
- ¹⁶ A. A. Lucas, H. Morawitz, G. R. Henry, J.-P. Vigneron, P. Lambin, P. H. Cutler, and T. E. Feuchtwang, *Physical Review B* **37**, 10708 (1988).
- ¹⁷ G. Doyen, D. Drakova, and M. Scheffler, *Physical Review B* **47**, 9778 (1993).
- ¹⁸ A. Mayer and J.-P. Vigneron, *Physical Review B* **56**, 12599 (1997).
- ¹⁹ A. Mayer and J.-P. Vigneron, *Journal of Vacuum Science & Technology B* **17**, 506 (1999).
- ²⁰ A. Mayer, M. S. Chung, B. L. Weiss, N. M. Miskovsky, and P. H. Cutler, *Physical Review B* **77**, 1 (2008).
- ²¹ N. M. Miskovsky, S. J. Shepherd, P. H. Cutler, T. E. Sullivan, and A. A. Lucas, *Applied Physics Letters* **35**, 560 (1979).
- ²² Y. Kuk, R. S. Becker, P. J. Silverman, and G. P. Kochanski, *Physical Review Letters* **65**, 456 (1990).
- ²³ A. V. Bragas, S. M. Landi, and O. E. Martínez, *Applied Physics Letters* **72**, 2075 (1998).
- ²⁴ X. W. Tu, J. H. Lee, and W. Ho, *Journal of Chemical Physics* **124**, 5 (2006).
- ²⁵ M. Dagenais, K. Choi, F. Yesilkoy, A. N. Chryssis, and M. C. Peckerar, *Energy* **7605**, 76050E (2010).
- ²⁶ D. R. Ward, F. Hüser, F. Pauly, J. C. Cuevas, and D. Natelson, *Nature nanotechnology* **5**, 732 (2010).
- ²⁷ B. Ricco and M. Y. Azbel, *Physical Review B* **29**, 1970 (1984).
- ²⁸ T. Laloyaux, I. Derycke, J.-P. Vigneron, P. Lambin, and A. A. Lucas, *Physical Review B* **47**, 7508 (1993).
- ²⁹ A. Mayer and P. Lambin, *Nanotechnology* **16**, 2685 (2005).
- ³⁰ W. R. Smythe, *Static and dynamic electricity*, Vol. 3 (McGraw-Hill New York, 1950).
- ³¹ E. L. Murphy and R. H. Good, *Physical Review* **102**, 1464 (1956).
- ³² A. Modinos, *Solid-State Electronics* **45**, 809 (2001).
- ³³ A. Mayer and J.-P. Vigneron, *Physical Review E* **59**, 4659 (1999).
- ³⁴ J. B. Pendry, *Journal of Modern Optics* **41**, 209 (1994).
- ³⁵ A. Mayer, M. S. Chung, B. L. Weiss, N. M. Miskovsky, and P. H. Cutler, *Physical Review B* **78**, 1 (2008).
- ³⁶ M. Büttiker and R. Landauer, *Physical Review Letters* **49**, 1739 (1982).
- ³⁷ T. E. Sullivan, Y. Kuk, and P. H. Cutler, *IEEE Transactions on Electron Devices* **36**, 2659 (1989).
- ³⁸ A. Mayer and J.-P. Vigneron, *Physical Review B* **62**, 16138 (2000).
- ³⁹ N. M. Miskovsky, S. H. Park, P. H. Cutler, and T. E. Sullivan, *Journal of Vacuum Science and Technology B* **12**, 2148 (1994).

- ⁴⁰ J. P. Lu, *Physical Review Letters* **79**, 1297 (1997).
- ⁴¹ H. Jussila, H. Yang, N. Granqvist, and Z. Sun, *Optica* **3**, 151 (2016).
- ⁴² A. Mayer, M. S. Chung, B. L. Weiss, N. M. Miskovsky, and P. H. Cutler, *Nanotechnology* **21**, 145204 (2010).